ACS APPLIED MATERIALS & INTERFACES

www.acsami.org

Research Article

Formation of the Inorganic and Organic Shells on the Surface of CdSe Quantum Dots

Oleg N. Karpov, Galina N. Bondarenko, Alexey S. Merekalov, Georgiy A. Shandryuk, Olga M. Zhigalina, Dmitriy N. Khmelenin, Elena A. Skryleva, Leonid A. Golovan, and Raisa V. Talroze*

Cite This: *ACS Appl. Mater. Interfaces* 2021, 13, 36190–36200

Read Online

ACCESS | Metrics & More | Article Recommendations | Supporting Information

ABSTRACT: Embedding quantum dots (QDs) into an organic matrix of controllable order requires the identification of their structural characteristics. This analysis is necessary for the creation of anisotropic composites that are sensitive to external stimuli. We have studied the QD structures formed during the single-step synthesis of CdSe/ZnS QDs and their transformations after the initial ligand's substitution for another ligand. This single-step process leads to the formation of the core/shell structure. We detect the presence of two oleic acid residues ionically connected to Zn and Cd. At the same time, the amount of Cd oleate at the surface is very small. We observe the ligand exchange process at the surface of the core/shell QDs. The oleic acid residues are substituted by terphenyl-containing (TERPh-COOH) aromatic acid residues. The reaction between CdSe/ZnS carrying TOP and oleic acid residues ionically bound with QDs and terphenyl-containing acid leads to the coexistence of multiple ligands on the QD surface at a ratio of 11:6:33 for TOP/OA/TERPh-COOH.

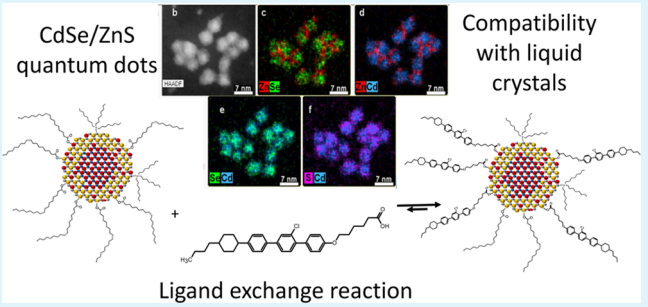

KEYWORDS: *quantum dot, core/shell, ligands exchange, liquid crystals, photoluminescence*

INTRODUCTION

Semiconductor quantum dots (QDs), their synthesis, modification, and applications are now considered as an integral part of modern materials science. The quantum confinement effect reflected in the size- and shape-dependent optical properties is responsible for the great attention of the scientific community.[1−6] There are several methods of the synthesis of quantum dots, which depend on the requirements for the materials under development. One may divide QDs into three general groups in accordance with the criterion of homogeneity of the radial distribution of atoms. The classical "core" group constitutes the first type of QDs. The second group consists of so-called "core/shell" structures in which the clear edge exists between the inner and outer areas containing different components. Shells stabilize the growth of QD cores and ensure the passivation of the core surface.[7−10] Talapin et al.[11] have reported on the synthesis and characterization of core/shell/shell nanocrystals. The middle shell, CdS, or ZnSe between the CdSe core and the ZnS shell leads to the reduction of the strain inside the nanoparticle between CdSe and ZnS due to the middle shell material having the lattice parameter intermediate to those of CdSe and ZnS. Chae et al.[12] have investigated the three-dimensional structure of core/shell nanocrystals by means of high-resolution scanning transmission electron microscopy (HRTEM), STEM, and local electrode APT analysis in detail. The authors have come to the conclusion that the core/double-shell structure provides the most desirable properties of QDs, such as the defect-free shell and higher quantum yield of luminescence. Typically, the structures of the core/shell type may be prepared by a two-step synthesis when the core is formed during the first process and its coverage with the shell occurs in the second step. The major characteristics of the core and core/shell QDs are the homogeneity of the atomic structure at the surface of either core or just shell layers. A single-step synthetic method based on the difference in the reactivity between Cd and Zn and Se and S precursors results in the formation of the third group of QDs.[13−15] The latter is characterized by the gradual change of the composition when there is no clear radial interface between the core and the shell, and one could observe core atoms at the shell surface of a QD. The content of such groups at the surface may vary, and that is why the chemical properties of the QD surface can also change. It is particularly important if organic ligand molecules are used to prevent QDs from clumping and large aggregate formation. Moreover, the type of ligand has to be particularly important in such a case when QDs are placed in a certain functional medium. The right choice of ligands may provide a strong interaction of those with QD surfaces. The

Received: June 4, 2021
Accepted: July 12, 2021
Published: July 21, 2021

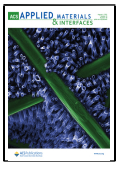

ACS Publications

© 2021 American Chemical Society

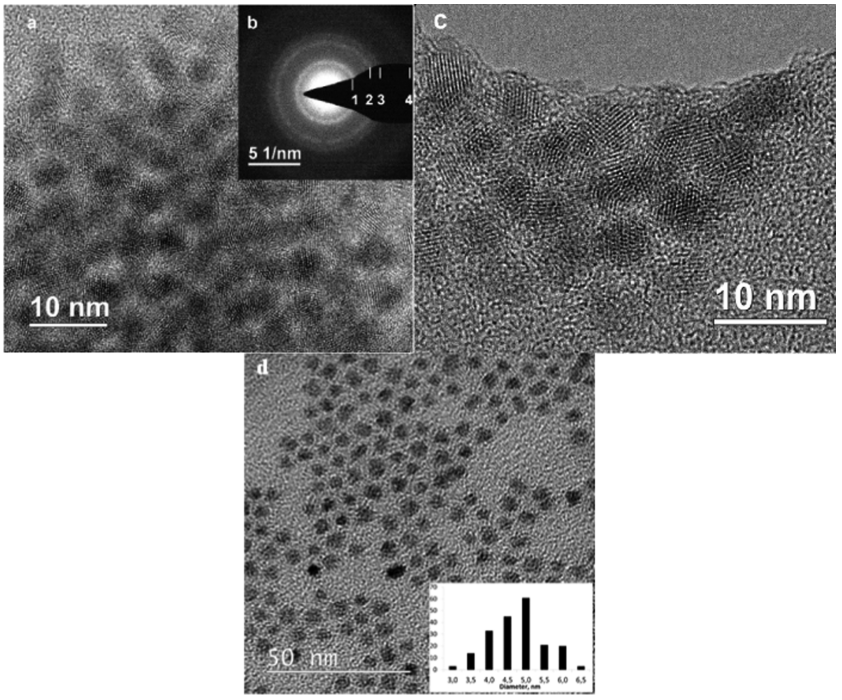

Figure 1. HRTEM images of the CdSe/ZnS QDs stabilized by oleic acid: (a, b) general view and SAED patterns. (c) Enlarged image of separated QDs and the TEM image (d).

most well-known ligands used for stabilization of QDs are tri-*n*-octyl phosphine oxide (TOPO), tri-*n*-octyl phosphine (TOP), oleic acid (OA), oleylamine (OAm), aromatic amines, thiols, etc.[16,17]

Due to particular optical and electronic properties, QDs are considered as active systems for application in different devices. One has to mention tunable photoluminescence related to the chemical structure and size of QDs and photochemical stability, which is superior in comparison to the organic dyes. As mentioned in the review of Cotta,[18] many commercial applications are available, and it is particularly true for QDs incorporated in display technology.[19] There are different QDs that are known as materials for a tunable spectral range of LEDs.[20−23]

Our research interests are mostly in creating new materials based on nanoparticles embedded into a functional matrix. One of the examples of such a matrix is a liquid crystal. During the last couple of decades, the experimental studies of liquid crystals are directed at the analysis of the role of inorganic NPs embedded in the LC matrix on the structure and phase behavior of liquid crystals as well as their future applications. Lots of information on that topic can be found in the review of Shen and Dierking[24] and references therein. Doping of a liquid crystal with QDs allows manipulating the optical, electro-optical, and alignment properties of liquid crystalline materials.[25−27] Note that in most cases, the amount of doped QDs is low. It may be related to the limited compatibility of QDs with liquid crystals. This idea was confirmed in theoretical predictions of the thermodynamic behavior of nematic liquid crystals doped with quantum dots discussed by Osipov and Gorkunov.[28−30] According to our opinion, such incompatibility results from the difference in the structure of NPs and surrounding mesogenic molecules, and a phase separation in LC/NP mixtures may occur in different phases, including an isotropic one. However, we suppose that the embedding of QDs having the right chemical structure of organic ligands at the surface may increase their compatibility with the organic liquid crystal medium.

In that respect, the major goal of our paper is to study the aspects of the QD's organic shell composition and its relation with the inorganic shell structure and to determine the influence of ligand's structure on the properties of QDs embedded into a liquid crystal.

For the purpose of our research, we have selected core−shell CdSe/ZnS QDs synthesized in accordance with the synthesis method described in ref 10. Two different ligands were analyzed, namely, the aliphatic acid OA and the aromatic one—6-((4″)-((1*S*,4*R*)-4-butylcyclohexyl 2′-chloro-[1,1′:4′,1″-terphenyl]-4-yl)oxy)hexanoic acid (TERPh-COOH). If OA becomes the part of the ligand structure in the process of the QD synthesis, the choice of TERPh-COOH is dictated by the structure of a liquid crystal under the study, namely, 4″-((1*S*,4*R*)-4-butylcyclohexyl-2′-chloro-[1,1′:4′,1″-terphenyl]-4-ethoxy), which is based on terphenyl-containing molecules. Terphenyls are known to exhibit unique optical[31] and electronic[32] properties, which are used for the preparation of organic light-emitting diodes[33−35] and field transistors.[36] All of these make composites of terphenyls with QDs very important and useful.

RESULTS AND DISCUSSION

Structure of Inorganic Part of QDs. As discussed above, the various methods of QD synthesis may result in the difference in their structure. If two-step synthesis leads to the clear edge between the core and the shell and to the certain homogeneity of the surface, the one-step synthetic procedure may cause not only the gradual change in the composition of the inorganic part of QDs but also the inhomogeneity of the atom distribution at the upper layer of the shell. To compare the structure of the near-surface layers of QDs and their interaction with different ligands, we have prepared QDs using the procedure described in ref 14 as a single-step method.

https://doi.org/10.1021/acsami.1c10315
ACS Appl. Mater. Interfaces 2021, 13, 36190−36200

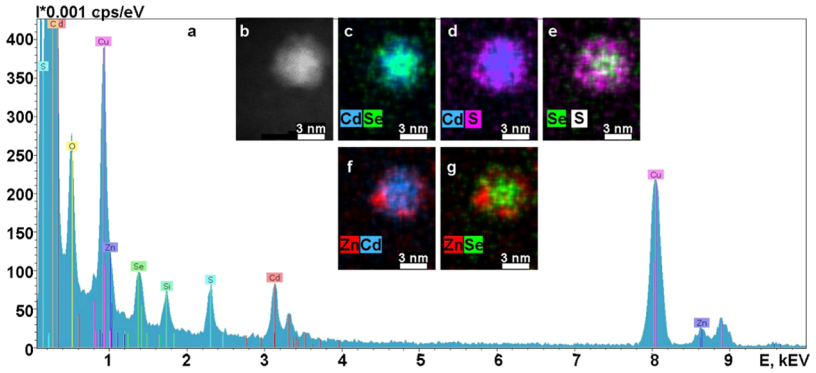

Figure 2. EDX spectra (a), STEM HAADF images with z-contrast for a single CdSe/ZnS NP (b), and the corresponding EDX mapping (c–g).

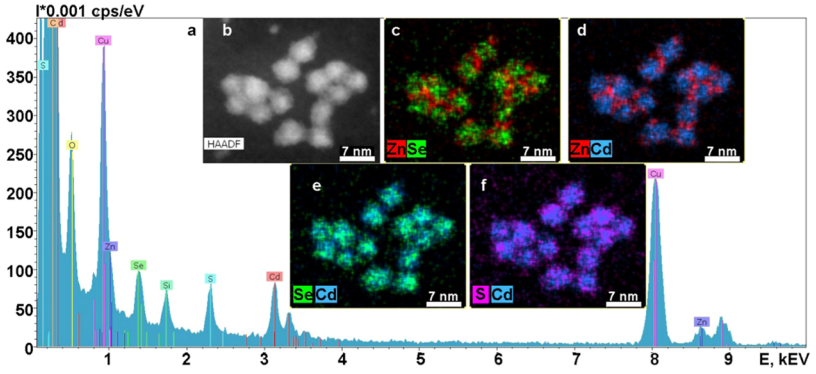

Figure 3. EDX spectra (a), STEM HAADF image with z-contrast for a group CdSe/ZnS NPs (b), and the corresponding EDX mapping (c–f).

At the first stage of our research, we have run the analysis of QDs by transmission electron microscopy (TEM), high-resolution electron microscopy (HRTEM), scanning transmission electron microscopy with a high-angle annular dark-field detector (HAADF STEM), electron diffraction (SAED), energy-dispersive analysis (EDA), and X-ray photoelectron spectroscopy (XPS). According to TEM data, QDs have a spherical shape of the average size of 4.5 nm (CdSe/ZnS) in diameter (Figure 1).

The set of interplanar spacing derived from the selected area electron diffraction SAED pattern (Figure 1b) with the values of 3.52, 2.14, 1.82, and 1.39 Å; correspond to *d*111, *d*220, *d*311, and *d*331, which in accordance with the crystal cell structure database correspond to CdSe having the cubic lattice, space group $F\bar{4}3m$ (19-0191 card).

At the same time, the Fourier diffraction patterns obtained from the individual NPs in HREM images indicate the presence of interplanar distances from phases that exist in smaller quantities, namely, ZnS–wurtzite, Zn with a hexagonal lattice (space group $P6_3/mmc$) and cubic CdS phases (space group $F\bar{4}3m$). Due to the small amount of these phases and the presence of organic ligands, we do not see rings corresponding to these phases in the electron diffraction patterns.

To visualize the distribution of chemical elements in quantum dots, HAADF STEM images and the corresponding elemental maps for an individual particle are obtained (Figure 2). Cadmium and selenium are located in the central part, and zinc and sulfur at the periphery of the particle. The same result can be seen for a group of particles (Figure 3). Note, however, that zinc and sulfur are not always located in the same way. Therefore, the presence of zinc in the form of a separate phase, as well as cadmium sulfide, cannot be ruled out (taking into account the Fourier analysis data). Based on the collected data, we may not consider a continuous homogeneous Zn–S shell of the same thickness formed on the CdSe core but a shell consisting of particles of zinc/zinc sulfide and cadmium sulfide. To a certain extent, one can view this type of shell structure as a gradual change of composition.

To further corroborate this idea, we have carried out the FTIR spectroscopy analysis of CdSe/ZnS QDs. The IR spectra show that the band ν_{CO} is split into two bands at 1547 and 1530 cm^{-1}. To assign these bands, the spectrum of CdSe/ZnS (3) stabilized by oleic acid is compared with those of Cd and Zn oleates (Figure 4).

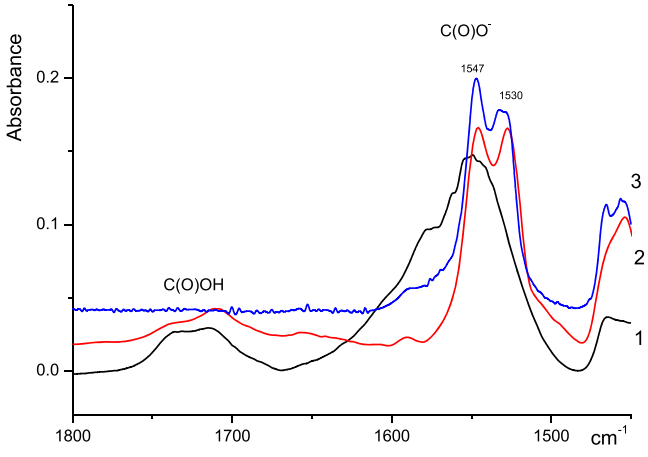

Figure 4. FTIR spectra: Cd oleate (1), Zn oleate (2), and CdSe/ZnS QDs stabilized by oleic acid (3).

https://doi.org/10.1021/acsami.1c10315
ACS Appl. Mater. Interfaces 2021, 13, 36190–36200

A fairly broad band at 1547 cm^{-1} related to the carboxylate anion attached to Cd^{2+} exists, whereas the spectrum of the carboxylate anion of Zn^{2+} contains two bands at 1531 and 1547 cm^{-1} with equal intensities. Although the same two bands are present in the spectrum of CdSe/ZnS QDs, the band at 1547 cm^{-1} is 9% more intense. Our estimations indicate the presence of about 91% Zn and 9% of Cd at the QD's surface.

Structure of the QD's Shell and Ligand Exchange. To compare the surface structure of the as-synthesized CdSe/ZnS QDs with that after surface modification of ligands with the new acid, containing terphenyl group, 6-((4″-((1*S*,4*R*)-4-butylcyclohexyl)-2′-chloro-[1,1′:4′,1″-terphenyl]-4-yl)oxy) hexanoic acid (TERPh-COOH, Scheme 1), we have run the ligand exchange reaction.

Scheme 1. Chemical Structure of TERPh-COOH

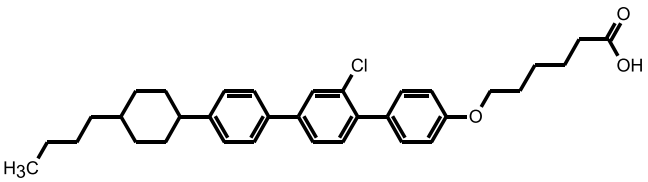

The reason for such a ligand exchange is described in the Introduction part. As we have shown in ref 37 with FTIR spectra, the treatment of QDs in sols with TERPh-COOH results in the substitution of OA acid on the surface of QDs, whereas the aromatic acid fragments appear (Scheme 2). However, questions arise about what ligands and in what amount are present at the surface after the ligand exchange.

In Figure 5, we present the results of the analysis of the elemental composition at the surface of CdSe/ZnS QDs carried out by XPS. The values of atomic concentration are given in Table 1. Using QUASES-IMFP-TPP2M software,[38] we have calculated the value of inelastic mean free pass (the distribution average distance covered by an electron between two inelastic shocks) and the value of the information depth (depth of analysis) in accordance with ref 39 at an emission angle of 45° and specified percentage of 95%.

This information depth is equal to 7−8 nm. Taking into account the size of CdSe/ZnS/TERPh-COOH QDs (4.5 ± 0.5 nm), we may conclude that the calculated value of the information depth captures both QD's core and shell, but with different attenuation, since the intensity of the photoelectron line decreases exponentially with depth. For this reason, the concentrations of the elements in the shell may be slightly overestimated, while the elements within the QD's core may be underestimated. That is why we use the data summarized in Table 1 for the comparison of the ratio of the carbon atom content to the sum of all element contents in QDs. This ratio in the sample CdSe/ZnS/TERPh-COOH becomes much higher than that in the sample of the as-synthesized QDs (CdSe/ZnS/TOP/OA). These results suggest the presence of aromatic acid fragments within the QD's shell. In addition, the appearance of chlorine (Cl) atom also supports this conclusion and even enables the estimation of the TERPh-COOH carbon content in the shell.

The direct proof for the presence of TOP at the surface would be the identification of the phosphorous element with XPS. However, the phosphorus peaks P 2p (131 eV) and P 2s (189 eV) that should be present in the sample CdSe/ZnS/TOP/OA overlap with intense selenium Auger peaks Se LMM. For this reason, it is not possible to estimate the P-element content by XPS.

Along with C and O elements characteristic of the organic shell, Cd, Se, Zn, and S signals appear, indicating that we analyze the elements inside the core−shell inorganic structure as well. Taking into account that the average diameter of CdSe/ZnS QDs is 4.5 nm, we conclude that the information received may be gathered from both inorganic parts and organic shells.

Using the known amounts of carbon and oxygen in OA and TOP, we applied the data of Table 1 to estimate the ratio between the amounts of OA and TOP ligands on the surface of QDs as synthesized, which is equal to 2.4:1. The analysis of TGA data presented in Figure S1 shows that the total amount of organic shell is about 30 wt % of the total mass of QDs. Considering the presence of peaks related to the degradation of organic molecules of two types, we have estimated the ratio

Scheme 2. Illustration of the Ligand Exchange Reaction on CdSe/ZnS Core−Shell QDs

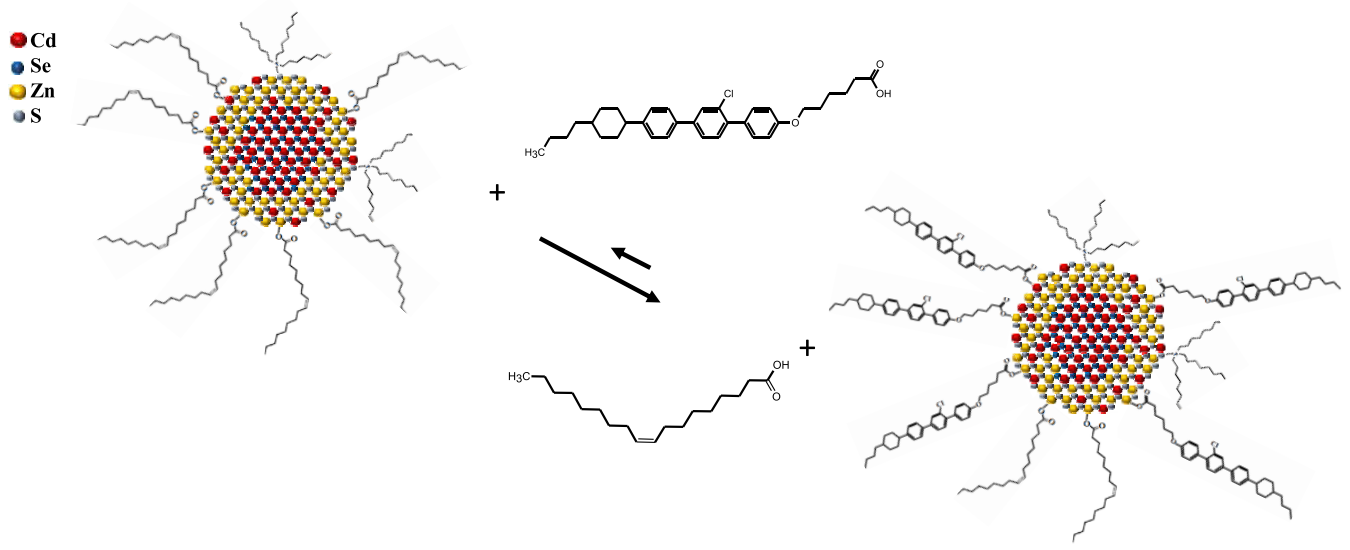

https://doi.org/10.1021/acsami.1c10315
ACS Appl. Mater. Interfaces 2021, 13, 36190−36200

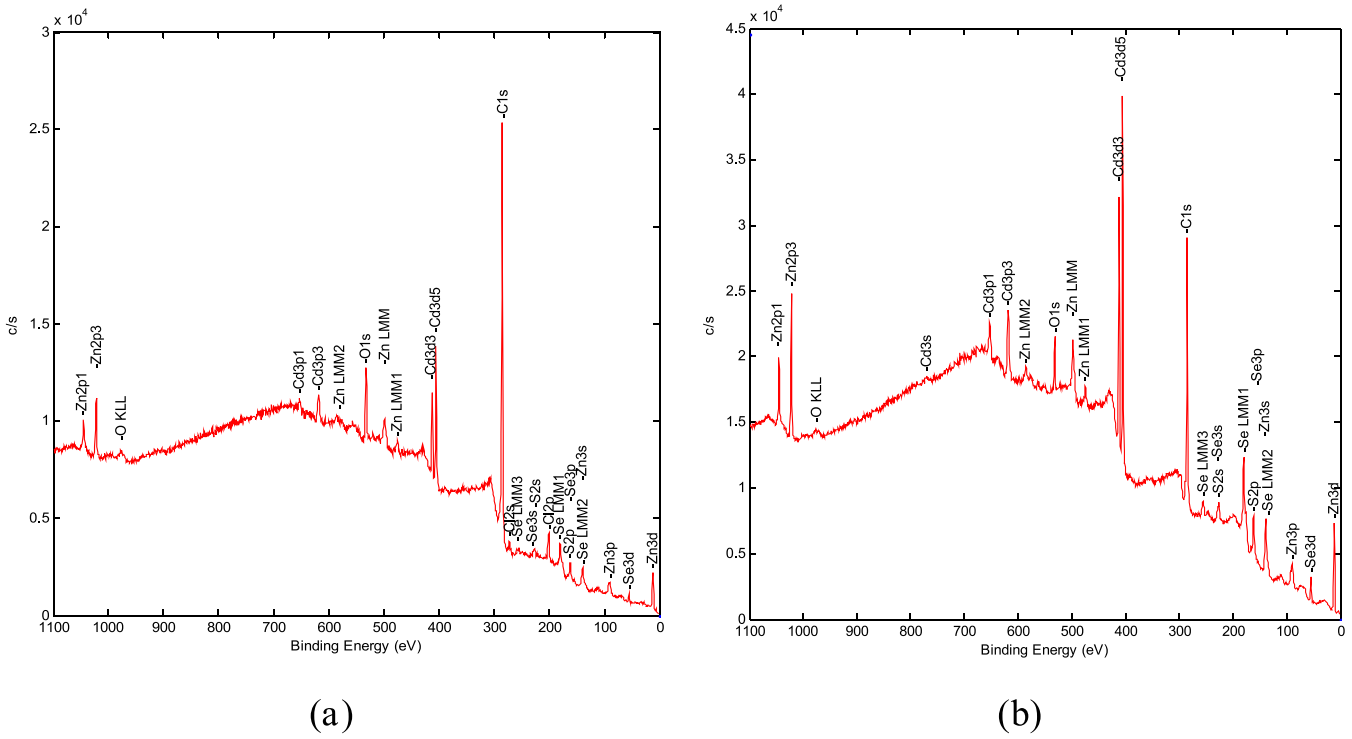

Figure 5. Survey spectra of CdSe/ZnS QDs before (a) and after (b) ligand exchange.

Table 1. Concentration of Elements (at. %)

	element							
sample	C ± 1.0	O ± 0.3	Cd ± 0.3	Se ± 0.1	Zn ± 0.2	S ± 0.7	Cl ± 0.2	C/(Cd + Se + Zn + S)
CdSe/ZnS/TOP/OA	78.0	5.6	5.3	2.1	4.2	4.8[a]	–	4.8
CdSe/ZnS/TERPh-COOH	86.1	6.4	1.6	0.6	1.6	1.8[a]	1.9	15.4

[a]– Se peaks overlap with S 2p and S 2s sulfur peaks. We calculated the S content with S (2s) because the contribution of Se (3s) is not too high, though the S concentration may be overestimated.

between the molecular fractions of OA and TOP at the surface of QDs to be 2.9:1 before the ligand exchange.

The same estimation is carried out, but also taking into account the presence of Cl for the QDs after ligand exchange. As it shows, the ratio between the amount of molecules on the surface is TERPh-COOH/OA/TOP = 5.4:1:1.8. All of these data confirm at least the partial ligand exchange.

The shape of the C 1s spectrum changes as well. Figure 6 presents the original C 1s spectra of two samples, which are different in the width of the main peak and in the higher energy part of the spectrum.

Moreover, the replacement of aliphatic ligands by aromatic ones has to be accompanied by the appearance of the shake-up peak shifted by 6−6.5 eV. The spectrum of the as-synthesized sample does not contain this peak, although it appears in the spectrum after the ligand exchange. The approximation of the spectra procedure shows the difference in the basic peak (Table 2), which is present in the spectrum of CdSe/ZnS/TOP + OA as a single peak with the binding energy at 285.2 eV and with a weak one at 288.9 eV. The assignment of peaks with the database[40] gives the following: peak 1, carbon atoms in phenyl rings without heteroatoms; peak 2, carbon atoms in aliphatic groups; peak 3, one C atom in the phenyl ring functionalized with a chlorine (Cl) atom plus 2 atoms connected with O (C−O); and peak 4, a C atom in the COO group.

The fitting of the CdSe/ZnS/TERPh-COOH spectrum allows for highlighting the peaks in the basic part of the spectrum: peak 1 at 284.7 eV is characteristic of carbon in the aromatic structures. The position of the second peak changes under fitting at 285.2 eV (Table 2). This peak is associated with the carbon atoms in the aliphatic ligands. Peak 4 is the same as in the initial as-synthesized sample corresponding to the COO group (the shift regarding peak 2 is 3.9 eV), and a new peak 3 appears, which is related to the C−O−C bond.

Considering the ratio between the number of elements in the organic shell given in Table 1, we have recalculated the content of aliphatic and aromatic carbon atoms in the first and second samples. We have found that the content of aliphatic carbon atoms in CdSe/ZnS (as synthesized) is 97 at. %, whereas in CdSe/ZnS, after the ligand exchange, the same carbon atoms are present in an amount of 55.4 at. % and the aromatic carbon is presented in an amount of 41 at. %. The comparison numbers mentioned above with those summarized in Table 1 show that the experimentally measured C content is in good agreement with the theoretical calculations.

Note that the structure identified by FTIR[37] changes substantially after the ligand exchange reaction (Scheme 2). The presence of the carboxylic group in TERPh-COOH is confirmed by an intense band at 1699 cm^{-1} induced by stretching of the C═O group in the FTIR spectrum. This band is completely absent in the spectra of QDs modified by TERPh-

https://doi.org/10.1021/acsami.1c10315
ACS Appl. Mater. Interfaces 2021, 13, 36190−36200

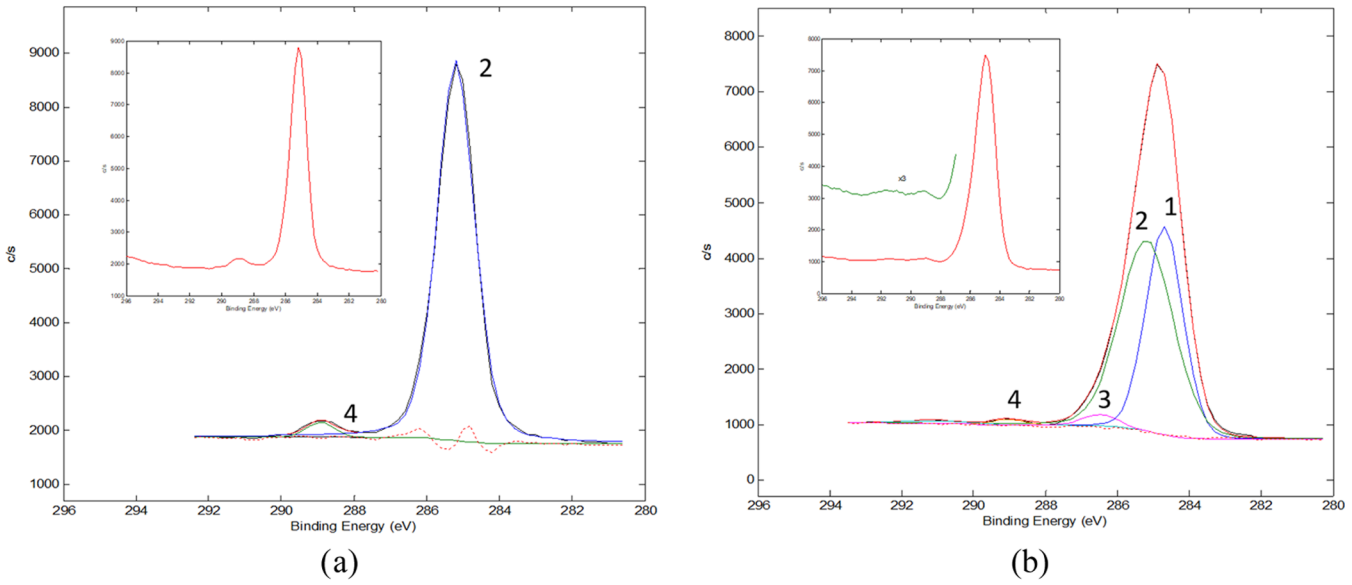

Figure 6. C 1s spectra of CdSe/ZnS/TOP + OA (a) and CdSe/ZnS/TERPh-COOH (b) after the fitting procedure. Insets show the corresponding original spectra. The number of peaks corresponds to those in Table 2.

Table 2. Parameters of the C 1s Spectra

sample	parameters	1	2	3	4	shake-up
CdSeZnS/TOP + OA	$E_B \pm 0.2$ eV		285.2		288.9	
	FWHM, eV		1.22		0.94	
	relative intensity ± 5, %		97		3	
CdSe/ZnS/TERPh-COOH	$E_B \pm 0.2$ eV	284.7	285.2	286.5	289.0	291.2
	FWHM, eV	1.22	1.77	1.14	0.9	2.0
	relative intensity ± 5, %	41	55.4	2.0	0.7	0.9

COOH (Figure 7). At the same time, the stretching of C−C bonds in phenyl rings at 1605 and 1524 cm^{-1} as well as the bands related to the C−H bending (1460−1470 cm^{-1}) are present in the spectra of both the acid and the QDs. Moreover, a new band at 1538 cm^{-1} appears in the spectra of QDs (as a shoulder in spectrum 2). Bands in that region (1500−1600 cm^{-1}) are characteristic of C═O stretching in carboxylate anions COO^-. It means that TERPh-COOH acid undergoes the transformation to the salt form after being bound to the surface of QDs.

Going back to the XPS data regarding the ratio between the aromatic and aliphatic carbon atoms, a question should be asked as to why TERPh-COOH exhibits preferential adsorption even though it seems to have more steric hindrances than the OA fragment. To answer this question, we have additionally analyzed FTIR spectra, which show the strong changes in the conformation of the QD-bound TERPh fragment in comparison with TERPh-COOH participated in the reaction of the ligand exchange. The band at 932 cm^{-1}, which is related to the H−O−C angle deformation in the carboxylic group, disappears in the spectra of QDs modified by TERPh-COOH. The band at 1292 cm^{-1} corresponding to the O═C−O angle deformation changes its shape. The spectral bands related to C(Ph)−O at 1238 cm^{-1} and in the range of 1000−1050 cm^{-1} (C(Alk)−O bond) change their intensity and positions.

The changes in the angles accompanied by small energy costs may occur in these structural C−O−C nodes. Such changes will lead to the rotation of the TERPh fragment of the molecule and alter the conformation in the terminal alkyl fragment with the participation of the cyclohexane ring. Large changes in the

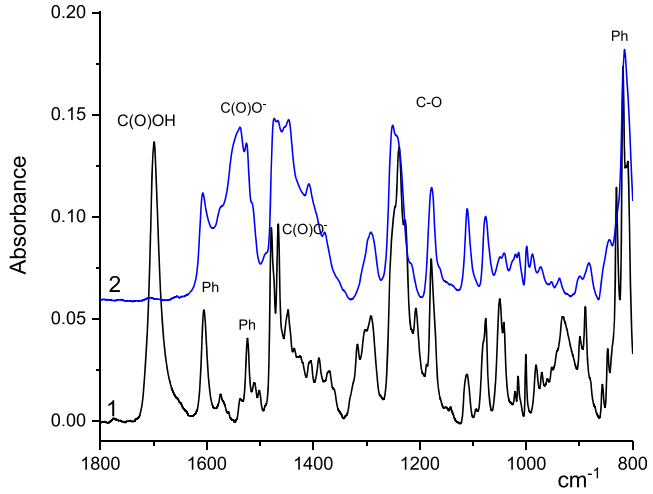

Figure 7. FTIR spectra of TERPh-COOH (1) and CdSe/ZnS QDs after ligand exchange (2).

spectrum are also observed in the range of 816−850 cm^{-1}, where bending vibrations of the H−C−C angles in 1,4 and 1,2,4-substituted aromatic rings are located. Usually, these bands are reliable reference points for sensing changes in the dihedral angles between the rings. That is why the position of the TERPh ligand around QDs may change the packing of TERPh-ligand fragments at the surface.

Thus, the general analysis of FTIR of all spectral signs of the participation of the entire TERPh fragment attached via the carboxylate group to the QD is evident. It includes the

https://doi.org/10.1021/acsami.1c10315
ACS Appl. Mater. Interfaces 2021, 13, 36190−36200

inclination toward the QD surface with a change in conformation and possibly π-coordination. It may provide a higher amount of TERPh fragments at the QD surface than OA molecules.

Comparison of Optical Properties of CdSe/ZnS QDs Bearing OA and TERPh-COOH Ligands. Absorption spectra and related PL spectra of CdSe/ZnS QDs as synthesized (a) and after ligand exchange (b) in toluene sols are shown in Figure 8.

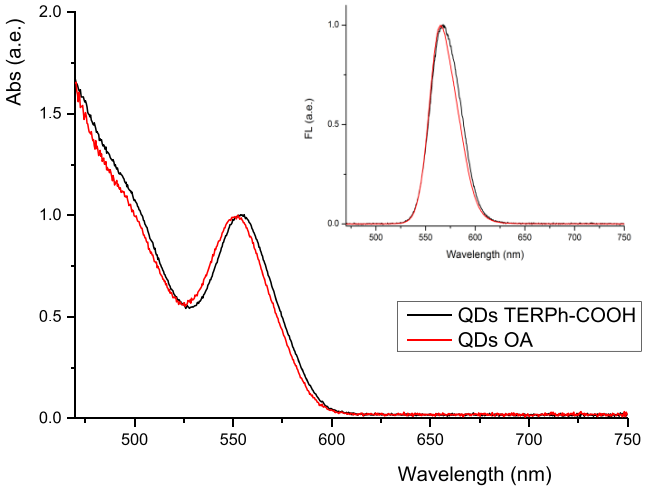

Figure 8. UV−vis absorption and PL spectra of CdSe/ZnS QDs stabilized by OA acid (red) and after ligand exchange with TERPh = COOH (black) in toluene sol.

The position of the UV−vis spectral band as well as PL spectra do not change appreciably upon the ligand exchange. Further information is obtained from the PL kinetics analysis (Figure 9). In addition to the major short wavelength band (565−600 nm) related to exciton recombination, one can detect the long-wavelength band (700−800 nm) caused by radiative recombination at V_{Se} traps. The latter band demonstrates two-order-of-magnitude less intensity than the first one. Comparison of the exciton bands suggests a 4 nm less bandwidth for the case of aromatic ligands. The QDs with aromatic ligands show a relatively small contribution of the trap band than in QDs with aliphatic ligands. This fact indicates lower amounts of traps in the QDs with aromatic ligands.

In both cases, the PL kinetics of the exciton band is well described by the sum of two decaying exponents

$$I_{PL}(t) = A_1 \exp\left(-\frac{t}{\tau_1}\right) + A_2 \exp\left(-\frac{t}{\tau_2}\right)$$

The parameter values for the exciton band found as a result of fitting are shown in Table 3. As one can see, in the case of aliphatic ligands, time constant τ_2 is insignificantly less than the one in the case of aromatic ligands.

Table 3. Parameter Values for the Exciton Bands

QD ligand	A_1/A_2	τ_1	τ_2
aliphatic	10.9 ± 1.1	20 ± 1	71 ± 4
aromatic	9.8 ± 1.0	21 ± 1	83 ± 5

There is a very small difference between the aliphatic and aromatic ligands. We may assume that the tiny narrowing of the PL band and a slight change of one of the time constants result from the more efficient passivation of traps by aromatic ligands. The latter may cause the smaller amount of excitons captured by traps (the narrowing of the band), with a smaller rate (the increase in time), etc. However, the difference is so insignificant that it is hard to discern the effect of two different ligands on the recombination of charge carriers.

According to various publications, the replacement of an organic ligand at QD's surface by a different molecule may provide an increase in some parameters of PL, for instance, quantum yield and lifetime of the excited state.[41] On the other hand, it may cause quite the opposite effect.[42] It is evident that a different variant exists when the change in the structure of the organic ligand shell does not really contribute to QD's PL. The latter seems to be the case under our consideration. However, this is related to the optical properties of QDs with ligands of different chemical structures, whereas an important role of those may be exhibited when QDs are embedded in functional media like liquid crystals.

Comparison of Thermal Behavior of Liquid Crystals Filled with QDs Bearing Different Ligands. As mentioned previously, the development of new materials allows for creating

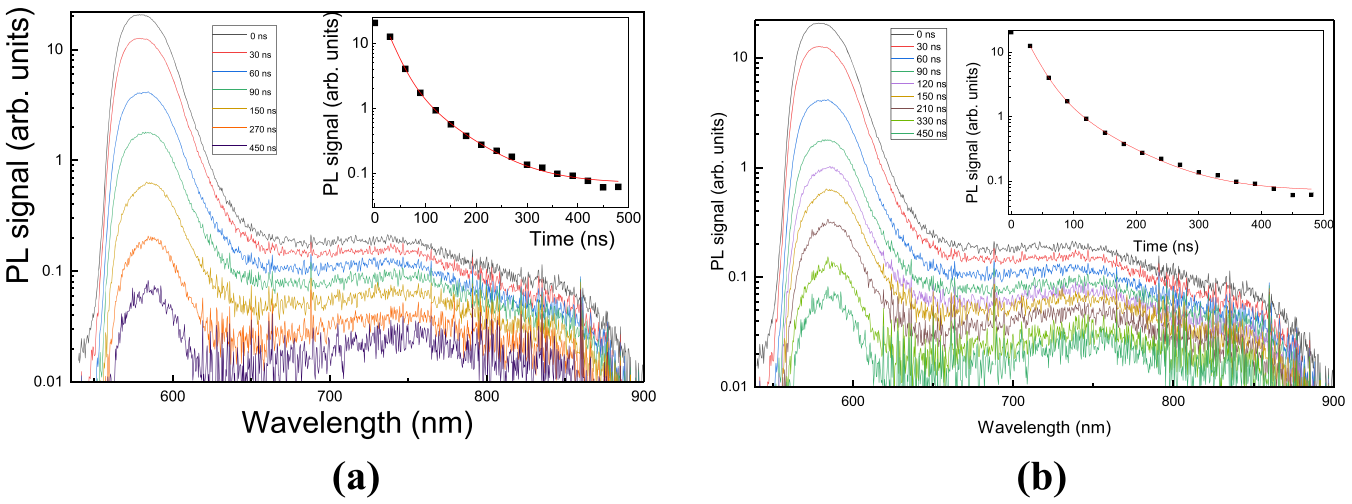

Figure 9. PL spectra and kinetics of exciton relaxation of QDs stabilized with OA (a) and TERPh-COOH (b) in toluene sols.

https://doi.org/10.1021/acsami.1c10315
ACS Appl. Mater. Interfaces 2021, 13, 36190−36200

composites that exhibit the properties of liquid crystals (LCs) and inorganic nanoparticles. One of the important points of embedding QDs in LCs is the possibility to affect their electro-optical characteristics if QDs are compatible to some extent with the LC medium. The latter is directly related to the nematic−isotropic phase transition temperature (T_{NI}). Osipov and Gorkunov[28,30] explained the effect of T_{NI} drop with the increasing content of QDs as a dilution effect when QDs have isotropic shape and predicted the possible increase in that transition temperature for systems filled with QDs of anisotropic shape.

To determine the influence of ligands on the T_{NI} transition, we have chosen the liquid crystal 4″-((1*S*,4*R*)-4-butylcyclohexyl-2′-chloro-[1,1′:4′,1″-terphenyl]-4-ethoxy),[43] which has a chemical structure very similar to that of TERPh-COOH. In Figure S2, we show representative DSC scans of the above liquid crystal (curve 1) doped with TERPh-COOH QDs (curve 2) and QDs having OA ligands (curve 3).

The doping of the liquid crystal matrix with OA and TERPh-COOH-functionalized CdSe/ZnS QDs results in a noticeable difference in the T_{NI} with the increasing content of QDs (Figure 10).

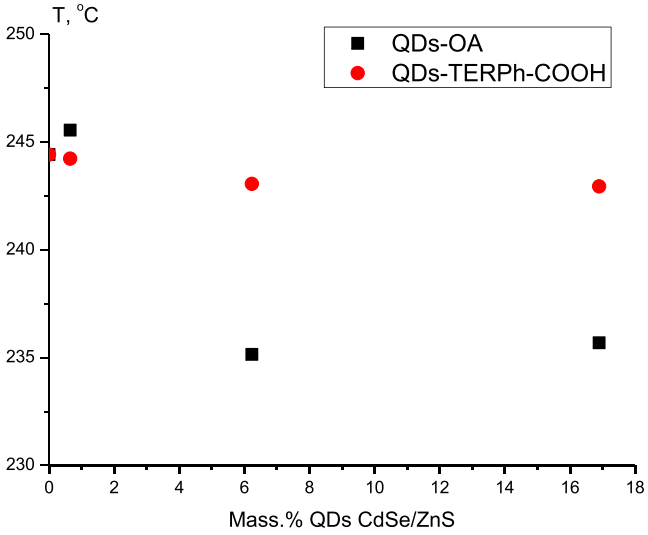

Figure 10. Nematic−isotropic phase transition temperature as a function of QD content.

If one uses QDs with OA ligands, the T_{NI} of the liquid crystal drops down by about 10° for 5 mass. % content of QDs, whereas the addition of QDs having TERPh-COOH ligands makes the decrease in the liquid crystal T_{NI} almost negligible. The profile of the LC system for T_{NI} of OA-stabilized QDs as a function of concentration is similar to that shown and discussed in ref 30, albeit there is a strong quantitative difference exceeding the theoretical estimates. A strong depression of the transition temperature was discussed in ref 44 as a result of the dilution effect and possible destabilization of orientational order in the vicinity of QDs. At the same time, even the partial substitution of OA ligands by terphenyl derivative completely changes the situation, and the negligible change in T_{NI} may occur with the lesser destabilization of order due to the very similar chemical structure of the ligand and terphenyl-based liquid crystal, resulting in a stronger interaction of ligands with LC medium. This approach indicates the possibility of increasing the compatibility of QDs with liquid crystal medium if the right ligand is chosen.

CONCLUSIONS

Using TEM, HRTEM, HAADF STEM, and EDA techniques in combination with XPS and FTIR analyses, we have shown that the single-step process that we have used for the synthesis of CdSe/ZnS QDs leads to the chemical composition gradient. It results in the appearance of core CD atoms in the shell, possibly close to the surface. Simultaneously, it affects the structure of the organic shell. The formation of two oleic acid residues ionically connected to Zn and Cd is detected, although the amount of Cd salt at the surface is fairly small (~9%), whereas the amount of Zn oleate is 91% of all oleic acid ligands at the surface. The XPS method allowed us to determine the ratio of OA fragments and TOP molecules at the surface of CdSe/ZnS QDs: 29% of TOP molecules and 71% OA residues. We confirm the ligand exchange process at the surface of core/shell QDs via substitution of oleic acid by the aromatic terphenyl-containing acid. As expected, the ligand exchange process cannot induce full substitution. Now it is clear that the OA residues still left at the surface are present in the amount of 12%, the amount of TOP is 22%, but the major ligand is TERPh-COO^-, which appears at the surface in the amount of 66%. The optical properties of QDs in solutions and thermal properties in a liquid crystal show that the chemical structure of QD ligands does not contribute much to photoluminescence and its kinetics. However, the nematic−isotropic phase transition temperature is sensitive to QD ligands if QDs are embedded in a liquid crystal. The quantitative effect of the QD content has to influence the functional parameters of liquid crystals such as voltage control, viscosity, dynamics of relaxation, switch-on and switch-off times, and orientation of a liquid crystal. Contrary to what is known today, the amount of QDs inserted in the LC media is limited by 0.1−0.25 wt %,[25,27,45,46] whereas we have shown that changing the ligand structure making it more similar to the liquid crystal one allows increasing the QD content about 1 order of magnitude and even more. The latter observation proves the necessity of analyzing the role of QDs in the thermal and thermodynamic behavior of blends when organic ligands are exchanged. It may strongly affect the miscibility of QDs with a functional medium influencing the LC response to the external fields. The results obtained indicate the trend of improving the material parameters for better performance of liquid crystals as materials for modern application in the field of optics, emission, LEDs, lasing, and colorimetric sensing.

EXPERIMENTAL SECTION

We received all commercially available starting materials, solvents, and reagents from Acros, Sigma-Aldrich, and Merck. The terphenyl-containing 6-((4″-((1*S*,4*R*)-4-butylcyclohexyl)-2′-chloro-[1,1′:4′,1″-terphenyl]-4-yl)oxy) hexanoic acid (TERPh-COOH) and 4″-((1*S*,4*R*)-4-butylcyclohexyl-2′-chloro-[1,1′:4′,1″-terphenyl]-4-ethoxy) was provided by prof. Vladimir Bezborodov team from the Department of Organic Chemistry, Belarusian State Technological University.

The synthesis of CdSe/ZnS QDs was carried out in accordance with ref 14 with the use of cadmium oxide (0.4 mmol), zinc acetate (4 mmol), and oleic acid (17.6 mmol). The reagents were mixed with 20 mL of 1-octadecene. The reaction mixture was gradually heated in a flow of argon under intense stirring till the total dissolution. After that, the mixture was heated up to 280 °C in an argon atmosphere and the solution of 0.4 mmol of selenium and 4 mmol of sulfur powder dissolved in 3 mL of TOP was injected. Then, the reaction mixture was maintained at high temperature for 5 min and rapidly cooled down to

https://doi.org/10.1021/acsami.1c10315
ACS Appl. Mater. Interfaces 2021, 13, 36190−36200

room temperature to stop the growth of QDs. The reaction mixture was divided into 5 equal parts, and 15 mL of acetone was added to each part. After that, each part was centrifuged it for 10 min at 6000 rpm. After that step, the precipitates were separated, brought together, and dissolved in 5 mL of toluene. To purify QDs, the reprecipitation was done three times by adding 15 mL of acetone.

Exchange of QD's Ligands. A total of 0.058 g of TERPh-COOH was dissolved in 0.5 mL of THF. Then, 0.01 g of CdSe/ZnS QDs was dispersed in 1 mL of THF and this sol was added slowly drop by drop to the TERPh-COOH solution. The mixture was maintained at room temperature for 72 h under stirring in an argon atmosphere. To clear from unreacted QDs and side products (OA), we reprecipitated the mixture in hexane and centrifuged for 10 min at 6000 rpm. The reaction mixture was added to 8 mL of hexane, and the red precipitate together with the colorless transparent solution was formed. The latter means the total possible binding of QDs with TERPh-COOH because QDs stabilized with OA are well dispersed in hexane. To extract the target product from the precipitate, the latter was dispersed in THF and hexane was added drop by drop (centrifuging after each portion) until the precipitation of the red QDs with modified ligands takes place. Unbound TERPh-COOH acid is left in the solution. The precipitate was dried under argon.

INSTRUMENTATION

FTIR spectra were registered with an ATR mode using an IR microscope HYPERION-2000 adjoint with a Fourier IR spectrometer IFS-66 v/s Bruker (50 scans, Ge crystal, 2 cm^{-1} resolution, 600−4000 cm^{-1} range).

Electron microscopy investigations of the structure and phase composition of the particles were carried out by transmission electron microscopy (TEM), high-resolution electron microscopy (HRTEM), scanning transmission electron microscopy with a high-angle annular dark-field detector (HAADF STEM), electron diffraction, and energy-dispersive analysis (EDA) in an FEI Tecnai Osiris microscope with an accelerating voltage of 200 kV. Elemental analysis and chemical element distribution mapping were performed on a special SuperX EDS system with four silicon detectors. The FEI Tecnai Osiris SuperX EDS system is designed to obtain rapidly (for several minutes) large area maps of chemical element distribution. Electron microscopy images were processed and analyzed with the Digital Micrograph, Esprit, TIA, and JEMS software.[47]

XPS spectra were recorded with a PHI5500 VersaProbe II XPS system. Al Kα X-ray excitation source ($h\nu$ = 1486.6 eV and 50 W power) was used to record the powder-like samples, which were pressed into indium support. We collected survey scans from the area of 200 μm in diameter. The analysis area diameter was 200 μm. The neutralizer was applied because of the strong surface charging due to low electrical conductivity of samples. The analysis of elements in at. % was carried out with the use of survey spectra measured with the method of relative element sensitivity factors. We used integral intensities of the following XPS spectra peaks: C 1s, O 1s, Cd 3d, Se 3d, Zn 3p, S 2s, and Cl 2p. The relative error of the peak intensity measurement does not exceed 10%. The binding energies, E_B, and photoelectronic were determined from high-resolution spectra taken at an analyzer transmission energy of 23.5 eV and the data collection density of 0.2 eV/step. The spectra were approximated using the nonlinear least-squares method using the Gauss−Lorentz function. The E_B scale was calibrated using Au 4f−83.96 eV and Cu 2p3−932.62 eV. Correction of the E_B scale was performed using the Cd 3d5 spectrum in CdSe, reference value −405.3 eV. The accuracy of determining the binding energy is ±0.2 eV.

The PL spectra of sols were registered by a USB 2000 spectrometer ("Ocean Optics") using hermetic glass optical cuvettes in the geometry close to 90°. The solutions of QDs and composites in "dry" toluene were purged with dry argon before measurements. Excitation sources were laser moduli with emission wavelengths of 403 nm and optical output power of 5−20 mW. The management software was SpectraSuite ("Ocean Optics"). All components of the measuring system were isolated from light.

Measurements of PL kinetics were carried out with excitation by the second harmonic of Nd:YAG laser radiation (EKSPLA PL 2143A, 532 nm, 25 ps, 10 Hz). The radiation was focused by the cylindrical lens into a 1 mm quartz cuvette filled with QD suspension in tetrahydrofuran. The PL spectra were recorded with the help of a Princeton Instruments Spectra Pro 2500i spectrometer (spectral resolution 0.8 nm) equipped with a gated multichannel amplifier and CCD array. The gate duration was set as 30 ns, and the spectra acquisition was carried out for 250 laser pulses. All measurements were performed at room temperature.

ASSOCIATED CONTENT

Supporting Information

The Supporting Information is available free of charge at https://pubs.acs.org/doi/10.1021/acsami.1c10315.

Results of TGA and DSC studies of the liquid crystals containing QDs (PDF)

AUTHOR INFORMATION

Corresponding Author

Raisa V. Talroze − *A.V. Topchiev Institute of Petrochemical Synthesis Russian Academy of Sciences, Moscow 119991, Russia*; orcid.org/0000-0002-9151-5493; Email: rtalroze@ips.ac.ru

Authors

Oleg N. Karpov − *A.V. Topchiev Institute of Petrochemical Synthesis Russian Academy of Sciences, Moscow 119991, Russia*

Galina N. Bondarenko − *A.V. Topchiev Institute of Petrochemical Synthesis Russian Academy of Sciences, Moscow 119991, Russia*

Alexey S. Merekalov − *A.V. Topchiev Institute of Petrochemical Synthesis Russian Academy of Sciences, Moscow 119991, Russia*

Georgiy A. Shandryuk − *A.V. Topchiev Institute of Petrochemical Synthesis Russian Academy of Sciences, Moscow 119991, Russia*

Olga M. Zhigalina − *Shubnikov Institute of Crystallography, Federal Research Center "Crystallography and Photonics", Russian Academy of Sciences, Moscow 119333, Russia; Bauman Moscow State Technical University, Moscow 105005, Russia*

Dmitriy N. Khmelenin − *Shubnikov Institute of Crystallography, Federal Research Center "Crystallography and Photonics", Russian Academy of Sciences, Moscow 119333, Russia*

Elena A. Skryleva − *National University of Science and Technology MISIS, Moscow 119049, Russia*

Leonid A. Golovan − *Faculty of Physics, M.V. Lomonosov Moscow State University, Moscow 119991, Russia*

Complete contact information is available at:

https://doi.org/10.1021/acsami.1c10315
ACS Appl. Mater. Interfaces 2021, 13, 36190−36200

https://pubs.acs.org/10.1021/acsami.1c10315

Author Contributions

This manuscript was written through contributions of all authors. All authors have given approval to the final version of the manuscript. All authors contributed equally.

Notes

The authors declare no competing financial interest.

■ ACKNOWLEDGMENTS

This research was funded by the Russian Science Foundation grant number 20-13-00341. The electron microscopy investigation was performed using the equipment of the Shared Research Center of Federal Scientific Research Center "Crystallography and Photonics" RAS. The study was supported by the Ministry of Science and Higher Education of the Russian Federation within a state assignment for the Federal Research Center "Crystallography and Photonics" of the Russian Academy of Sciences in the part concerning electron microscopy investigation.

■ REFERENCES

(1) Brus, L. Electronic Wave Functions in Semiconductor Clusters: Experiment and Theory. *J. Phys. Chem. A* **1986**, *90*, 2555−2560.
(2) Colvin, V. L.; Schlamp, M. C.; Alivisatos, A. P. Light-Emitting Diodes Made from Cadmium Selenide Nanocrystals and a Semiconducting Polymer. *Nature* **1994**, *370*, 354−357.
(3) Alivisatos, A. P. Semiconductor Clusters, Nanocrystals, and Quantum Dots. *Science* **1996**, *271*, 933−937.
(4) Murray, C. B.; Kagan, C. R.; Bawendi, M. G. Synthesis and Characterization of Monodisperse Nanocrystals and Close-Packed Nanocrystal Assemblies. *Annu. Rev. Mater. Sci.* **2000**, *30*, 545−610.
(5) Rogach, A. L.; Kornowski, A.; Gao, M.; Eychmueller, A.; Weller, H. Synthesis and Characterization of a Size Series of Extremely Small Thiol-Stabilized CdSe Nanocrystals. *J. Phys. Chem. B* **1999**, *103*, 3065−3069.
(6) Vasiliev, R. B.; Dorofeev, S. G.; Dirin, D. N.; Belov, D. A.; Kuznetsova, T. A. Synthesis and Optical Properties of PbSe and CdSe Colloidal Quantum Dots Capped with Oleic Acid. *Mendeleev Commun.* **2004**, *14*, 169−171.
(7) Reiss, P.; Protiere, M.; Li, L. Core/Shell Semiconductor Nanocrystals. *Small* **2009**, *5*, 154−168.
(8) Soni, U.; Arora, V.; Singh, G.; Hussain, M.; Sapra, S. *Synthesis of Core−Shell Quantum Dots and Their Potential Application*, Proceedings of the 2nd International Conference on Advanced Nanomaterials and Nanotechnology, Dec 8−10, 2011, Guwahati, India, 2013; pp 85−93.
(9) van Embden, J.; Jasieniak, J.; Mulvaney, P. Mapping the Optical Properties of CdSe/CdS Heterostructure Nanocrystals: The Effects of Core Size and Shell Thickness. *J. Am. Chem. Soc* **2009**, *131*, 14299−14309.
(10) Lim, J.; Bae, W. K.; Lee, D.; Nam, M. K.; Jung, J.; Lee, C.; Char, K.; Lee, S. InP@ZnSeS, Core@Composition Gradient Shell Quantum Dots with Enhanced Stability. *Chem. Mater.* **2011**, *23*, 4459−4463.
(11) Talapin, D. V.; Mekis, I.; Götzinger, S.; Kornowski, A.; Benson, O.; Weller, H. CdSe/CdS/ZnS and CdSe/ZnSe/ZnS Core−Shell−Shell Nanocrystals. *J. Phys. Chem. B* **2004**, *108*, 18826−18831.
(12) Chae, B. G.; Lee, J. H.; Park, S.; Lee, E.; Kwak, C. M.; Jafari, M.; Jeong, Y. R.; Park, C. G.; Seol, J.-B. Direct Three-Dimensional Observation of Core/Shell-Structured Quantum Dots with a Composition-Competitive Gradient. *ACS Nano* **2018**, *12*, 12109−12117.
(13) Dethlefsen, J. R.; Dossing, A. Preparation of a ZnS Shell on CdSe Quantum Dots Using a Single-Molecular ZnS Precursor. *Nano Lett.* **2011**, *11*, 1964−1969.
(14) Bae, W. K.; Char, K.; Hur, H.; Lee, S. Single-Step Synthesis of Quantum Dots with Chemical Composition Gradients. *Chem. Mater.* **2008**, *20*, 531−539.
(15) Zhang, W.; Zhang, H.; Feng, Y.; Zhong, X. Scalable Single-Step Noninjection Synthesis of High-Quality Core/Shell Quantum Dots with Emission Tunable from Violet to Near Infrared. *ACS Nano* **2012**, *6*, 11066−11073.
(16) Elimelech, O.; Aviv, O.; Oded, M.; Banin, U. A Tale of Tails: Thermodynamics of CdSe Nanocrystal Surface Ligand Exchange. *Nano Lett.* **2020**, *20*, 6396−6403.
(17) Drijvers, E.; De Roo, J.; Martins, J. C.; Infante, I.; Hens, Z. Ligand Displacement Exposes Binding Site Heterogeneity on CdSe Nanocrystal Surfaces. *Chem. Mater.* **2018**, *30*, 1178−1186.
(18) Cotta, M. A. Quantum Dots and Their Applications: What Lies Ahead? *ACS Appl. Nano Mater.* **2020**, *3*, 4920−4924.
(19) Shirasaki, Y.; Supran, G. J.; Bawendi, M. G.; Bulovic, V. Emergence of Colloidal Quantum-Dot Light-Emitting Technologies. *Nat. Photonics* **2013**, *7*, 13−23.
(20) Kim, Y.; Ham, S.; Jang, H.; Min, J. H.; Chung, H.; Lee, J.; Kim, D.; Jang, E. Bright and Uniform Green Light Emitting InP/ZnSe/ZnS Quantum Dots for Wide Color Gamut Displays. *ACS Appl. Nano Mater.* **2019**, *2*, 1496−1504.
(21) Cho, E.; Kim, T.; Choi, S.-M.; Jang, H.; Min, K.; Jang, E. Optical Characteristics of the Surface Defects in InP Colloidal Quantum Dots for Highly Efficient Light-Emitting Applications. *ACS Appl. Nano Mater.* **2018**, *1*, 7106−7114.
(22) Xu, X.; Zhou, L.; Ding, D.; Wang, Y.; Huang, J.; He, H.; Ye, Z. Silicene Quantum Dots Confined in Few-Layer Siloxene Nanosheets for Blue-Light-Emitting Diodes. *ACS Appl. Nano Mater.* **2020**, *3*, 538−546.
(23) Begum, R.; Chin, X. Y.; Damodaran, B.; Hooper, T. J. N.; Mhaisalkar, S.; Mathews, N. Cesium Lead Halide Perovskite Nanocrystals Prepared by Anion Exchange for Light-Emitting Diodes. *ACS Appl. Nano Mater.* **2020**, *3*, 1766−1774.
(24) Shen, Y.; Dierking, I. Perspectives in Liquid-Crystal-Aided Nanotechnology and Nanoscience. *Appl. Sci.* **2019**, *9*, No. 2512.
(25) Praseetha, K. P.; Divyasree, M. C.; Nimmy, J. V.; Chandrasekharan, K.; Varghese, S. Enhanced Optical Nonlinearity in Nematic Liquid Crystal on Doping with CdSe Quantum Dot. *J. Mol. Liq.* **2019**, *273*, 497−503.
(26) Tang, J.; Liu, F.; Lu, M.; Zhao, D. InP/ZnS Quantum Dots Doped Blue Phase Liquid Crystal with Wide Temperature Tange and Low Driving Voltage. *Sci. Rep.* **2020**, *10*, No. 18067.
(27) Konshina, E.; Shcherbinin, D.; Kurochkina, M. Comparison of the Properties of Nematic Liquid Crystals Doped with TiO2 and CdSe/ZnS Nanoparticles. *J. Mol. Liq.* **2018**, *267*, 308−314.
(28) Gorkunov, M. V.; Osipov, M. A. Mean-Field Theory of a Nematic Liquid Crystal Doped with Anisotropic Nanoparticles. *Soft Matter* **2011**, *7*, 4348−4354.
(29) Osipov, M. A.; Gorkunov, M. V. Molecular Theory of Phase Separation in Nematic Liquid Crystals Doped with Spherical Nanoparticles. *ChemPhysChem* **2014**, *15*, 1496−1501.
(30) Gorkunov, M. V.; Shandryuk, G. A.; Shatalova, A. M.; Kutergina, I. Y.; Merekalov, A. S.; Kudryavtsev, Y. V.; Talroze, R. V.; Osipov, M. A. Phase Separation Effects and the Nematic−Isotropic Transition in Polymer and Low Molecular Weight Liquid Crystals Doped with Nanoparticles. *Soft Matter* **2013**, *9*, 3578−3588.
(31) Todd, M. H.; Balasubramanian, S.; Abell, C. Studies on the Synthesis, Characterisation and Reactivity of Aromatic Diboronic Acids. *Tetrahedron Lett.* **1997**, *38*, 6781−6784.
(32) Udayakumar, B. S.; Schuster, G. B. Photoisomerization of 2,2″-ethano-bridged m-terphenyl Derivatives: Ring Constraint Activates an Unreactive Chromophore. *J. Org. Chem.* **1992**, *57*, 348−352.
(33) Wright, R. S.; Vinod, T. K. Synthesis of m-Terphenyl Derivatives for Potential Use as Tectons in Crystal Engineering. *Tetrahedron Lett.* **2003**, *44*, 7129−7132.
(34) Liao, H.-R.; Lin, Y.-J.; Chou, Y.-M.; Luo, F.-T.; Wang, B.-C. Theoretical Study of Optical and Electronic Properties of p-Terphenyls

Containing Cyano Substituents as Promising Light-Emitting Materials. *J. Lumin.* **2008**, *128*, 1373−1378.
(35) Garnier, F.; Hajlaoui, R.; Yassar, A.; Srivastava, P. All-Polymer Field-Effect Transistor Realized by Printing Techniques. *Science* **1994**, *265*, 1684−1686.
(36) Hide, F.; Diaz-Garcia, M. A.; Schwartz, B. J.; Heeger, A. J. New Developments in the Photonic Applications of Conjugated Polymers. *Acc. Chem. Res.* **1997**, *30*, 430−436.
(37) Bezborodov, V. S.; Finko, A. V.; Mikhalyonok, S. G.; Derikov, Y. I.; Shandryuk, G. A.; Kuz'menok, N. M.; Arol, A. S.; Karpov, O. N.; Talroze, R. V. Synthesis of New Mesomorphic Terphenyl Derivatives: the Influence of Terphenylene and Functional Fragments on the Mesomorphic Properties and Ligand Exchange on Quantum Dots. *Liq. Cryst.* **2021**, DOI: 10.1080/02678292.2021.1884912.
(38) *QUASES-IMFP-TPP2M Software*. http://www.quases.com/products/quases-imfp-tpp2m/ (accessed Aug 12, 2020).
(39) Powell, C. J. Practical Guide for Inelastic Mean Free Paths, Effective Attenuation Lengths, Mean Escape Depths, and Information Depths in x-Ray Photoelectron Spectroscopy. *J. Vac. Sci. Technol., A* **2020**, *38*, No. 023209.
(40) Beamson, G.; Brigs, D. *High Resolution XPS of Organic Polymers: The Scienta ESCA300 Database*; Wiley, 1992.
(41) Wang, L.; Lv, Y.; Ying, L.; Lin, J.; Zhao, J.; Liu, X.; Zeng, R.; Wang, X.; Zou, B. Surface Organic Ligand-Passivated Quantum Dots: Toward High-Performance Light-Emitting Diodes with Long Lifetimes. *J. Mater. Chem. C* **2021**, *9*, 2483−2490.
(42) Dayneko, S.; Lypenko, D.; Linkov, P.; Tameev, A.; Martynov, I.; Samokhvalov, P.; Chistyakov, A. Effect of Surface Ligands on the Performance of Organic Light-Emitting Diodes Containing Quantum Dots. *Proc. SPIE 9270* **2014**, *9270*, No. 927009.
(43) Bezborodov, V.; Dąbrowski, R.; Dziaduszek, J.; Czupryński, K.; Raszewski, Z. Synthesis and Physical Properties of Liquid Crystals Having a Chlorine Atom in the Lateral Position of a Benzene Ring. *Liq. Cryst.* **1996**, *20*, 1−8.
(44) Merekalov, A. S.; Shandryuk, G. A.; Bezborodov, V. S.; Otmakhova, O. A.; Mikhalyonok, S. G.; Kuz'menok, N. M.; Arol, A. S.; Osipov, M. A.; Talroze, R. V. Three in One: Mesogenic Aromatic Acid as a Liquid Crystal Matrix, a Chiral Dopant in Liquid Crystals and a Stabilizer for Nanoparticles. *J. Mol. Liq.* **2019**, *276*, 588−594.
(45) Rastogi, A.; Pathak, G.; Srivastava, A.; Herman, J.; Manohar, R. Cd_{1-X} Zn_XS/ZnS Core/Shell Quantum Dots in Nematic Liquid Crystals to Improve Material Parameter for Better Performance of Liquid Crystal Based Devices. *J. Mol. Liq.* **2018**, *255*, 93−101.
(46) Keshavarz, A.; Riahinasab, S. T.; Hirst, L. S.; Stokes, B. J. New Promesogenic Ligands for Host Medium Microencapsulation by Quantum Dots via Liquid Crystal Phase Transition Templating. *ACS Appl. Nano Mater.* **2019**, *2*, 2542−2547.
(47) Stadelmann, P. *JEMS*, 2015. http://www.jems-saas.ch.

https://doi.org/10.1021/acsami.1c10315
ACS Appl. Mater. Interfaces 2021, 13, 36190−36200